TRACE ELEMENTS AND OXYGEN ISOTOPES IN A CAI-BEARING MICRO-METEORITE FROM ANTARCTICA;

P. Hoppe, Physikalisches Institut, Universität Bern, Sidlerstr.5, CH-3012 Bern, Switzerland; G. Kurat and J. Walter, Naturhistorisches Museum, Postfach 417, A-1014 Vienna, Austria; M. Maurette, Centre de Spectrometrie Nucleaire et de Spectrometrie de Masse, Bâtiment 104, F-91405 Campus Orsay, France.

We continued our investigation of trace element abundances and oxygen isotopic compositions of spinel-rich CAIs in Antarctic micrometeorites. The particle studied is an unmelted phyllosilicate-rich micrometeorite which contains two spinel-rich CAIs. They consist of irregularly shaped Mg-Al-spinel which contain some small (< 2 µm) perovskite grains and are rimmed by a Fe-rich phyllosilicate. Both, spinel and the Fe-rich phyllosilicate rim, show flat chondrite-normalized patterns of the refractory trace elements which are strongly enriched by factors of ~ 200 and ~ 10 with respect to their CI abundances, respectively. The matrix has trace element contents that are chondritic for most elements with somewhat elevated abundances as compared to CI and CM chondrites. The spinel has oxygen isotopic compositions rich in ^{16}O (up to $\delta^{17,18}O$ of ~ -40‰) falling along or slightly to the ^{18}O-rich side of the carbonaceous chondrite anhydrous minerals mixing-line.

Particle MM94-4 #36 has an irregular shape and a diameter of about 100 µm. It contains two porous spinel bodies (~ 25 µm x 25 µm and ~ 50 µm x 15 µm) which enclose a few small perovskite and which are enveloped by a discontinuous rim of Fe-rich phyllosilicate with a thickness of up to 10µm. The chemical composition of the spinel is that of a Mg-Al-spinel containing minor amounts of SiO_2 (0.10 wt%), TiO_2 (0.19 wt%), Cr_2O_3 (0.16 wt%), and FeO (0.60 wt%) as determined by EMPA. Trace element abundances and oxygen isotopic compositions have been determined by SIMS. Trace element analyses were made with a 1-5 nA O^- primary beam (~ 10-20 µm), positive secondary ions, and energy filtering to supress interferences from complex molecular ions [1]. The oxygen isotopic analyses were made with a 10-50 pA Cs^+ primary beam (~ 3-5 µm) and negative secondary ions.

The trace element patterns of particle MM94-4 #36 are shown in Figs. 1a-c. Spinel has unfractionated refractory element abundances with enrichments of up to ~ 200x CI abundance in sp1 (Fig. 1a). The comparatively smaller refractory element enrichments of sp2 and sp3 can be attributed only in part to possible contributions from the surrounding matrix and phyllosilicate rim to the integrated secondary ion signals. Small deviations from the flat pattern are shown by Sc (depleted), Nb (enriched), and Eu (depleted). Among the less refractory elements V and Li are unusually abundant. The Fe-rich phyllosilicate rim has a trace element pattern (Fig. 1b) similar to that of spinel although the enrichments of the refractory elements (up to ~ 10x CI) are lower and Eu shows an anomaly of opposite sign. Trace element contents of the matrix are mostly chondritic, although slightly higher than those of CI and CM chondrites. Ba and Th are enriched up to 5-10x of their CI abundances, probably the result of terrestrial contamination.

The oxygen isotopic compositions of the matrix and of the Fe-rich phyllosilicate rim do not deviate significantly from the terrestrial fractionation line. Figure 2 shows the oxygen isotopic compositions of spinel in MM94-4 #36 along with the data previously obtained for spinels from two other Antarctic micrometeorites (MM92-15 #23, MM94-1 #28) [2], and Burma spinel for comparison (errors are 1σ). All micrometeoritic spinels are rich in ^{16}O with $\delta^{17,18}O$ of up to ~ -40‰ in MM94-4 #36 which comes close to the spinels from carbonaceous chondrites richest in ^{16}O [3] and a CAI found among interplanetary dust particles [4]. Three of our data points plot directly onto the carbonaceous chondrite anhydrous minerals mixing-line (CCAM) [3]. The remaining three data points fall on the ^{18}O-rich side of this line. Interestingly, these data points plot along the (extended) line found for spinel and hibonite in the Allende FUN inclusion EK1-4-1 [5].

The CAI of the present study is the first superrefractory inclusion identified in interplanetary dust to date. The differences in the trace element contents of the spinels indicate that the CAIs in MM94-4 #36 must be aggregates of spinels from different sources. The high V and possibly also Li abundances point to more oxydizing conditions during formation as compared to those of the carbonaceous chondrite CAI formation site. This confirms our previous conclusion for the MM92-15 #23 CAI [6]. On the other hand, the oxygen fugacity probably had not been high enough for Eu to be completely converted into the 3+ ionic state, as indicated by the negative Eu anomaly. The Fe-rich phyllosilicate rim replaces the commonly observed diopside rim and it probably formed by partial recondensation of a vapor escaping from the CAI during formation of the spinels. Its positive Eu anomaly apparently complements the Eu depletion of the spinel core. Oxygen has the isotopic pattern as known for CAIs from carbonaceous chondrites. However, the oxygen isotopic composition of spinel sp1 deviates significantly from the CCAM-line, indicating both nuclear effects (^{16}O-rich reservoir) and chemical fractionation during formation.

This work was supported by the Swiss National Science Foundation, the Austrian Fonds zur Förderung der wissenschaftlichen Forschung (project no. P8215-GEO), and by IN2P3 in France.

REFERENCES: [1] Zinner E. and Crozaz G. (1986) *Int. J. Mass Spectr. Ion Processes* **69**,17-38 [2] Kurat G. et al. (1994) *Meteoritics* **29**, 487-488. [3] Clayton R.N. (1993) *Ann. Rev. Earth Planet. Sci.* **21**, 115-149. [4] Stadermann F.J. (1991) *LPSC* **XXII**, 1311-1312. [5] Clayton R.N. and Mayeda T.K. (1977) *Geophys. Res. Lett.* **4**, 295-298. [6] Kurat G. et al. (1994) *LPSC* **XXV**, 763-764.

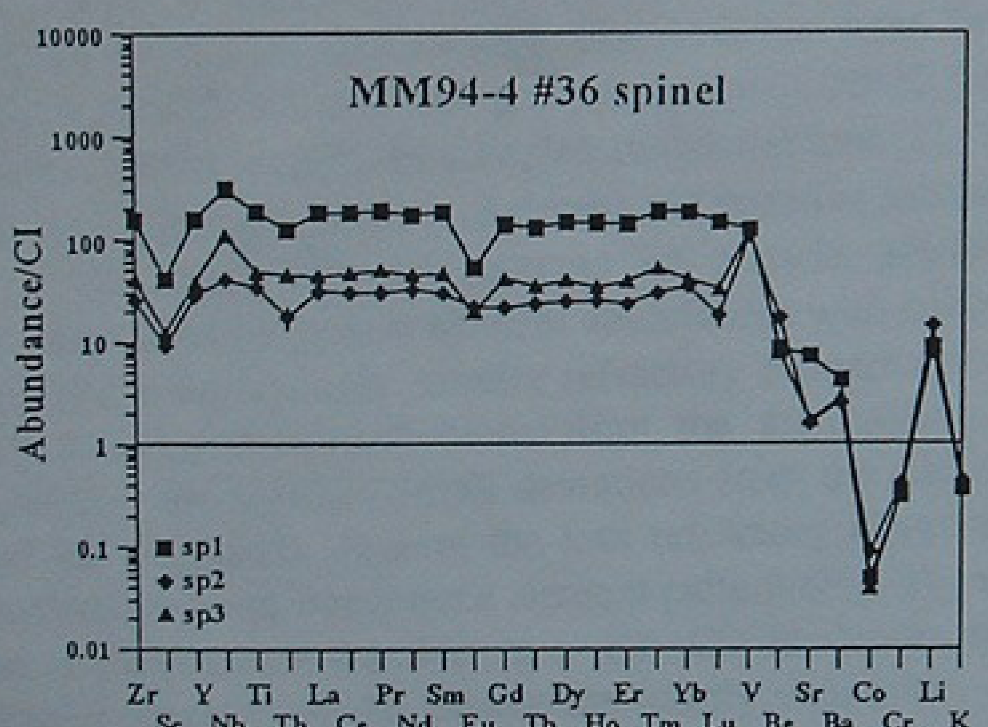

Figure 1a

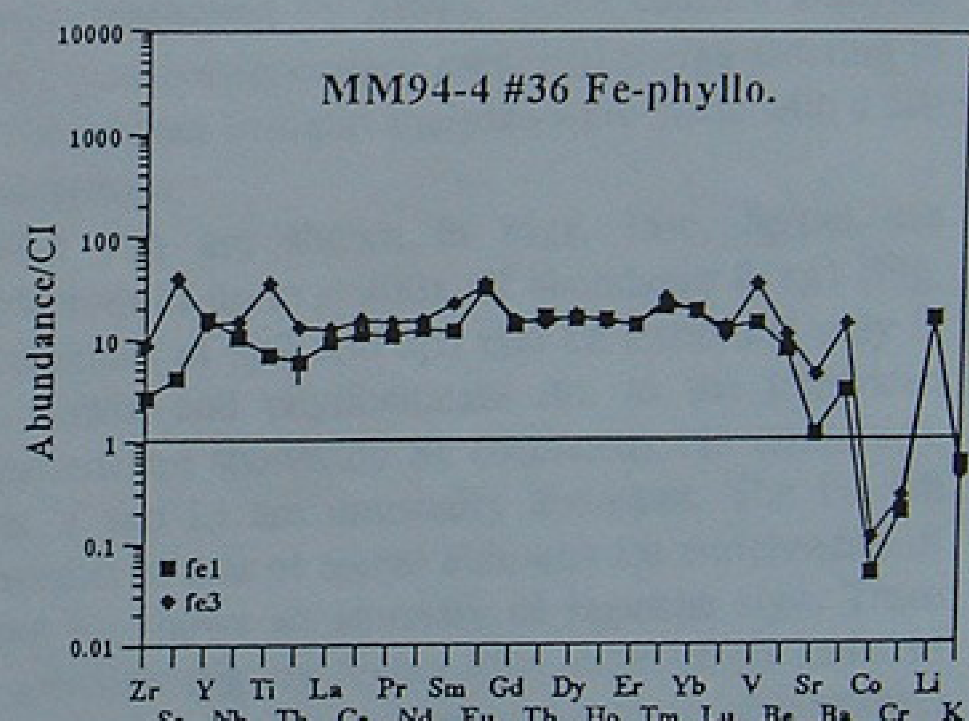

Figure 1b

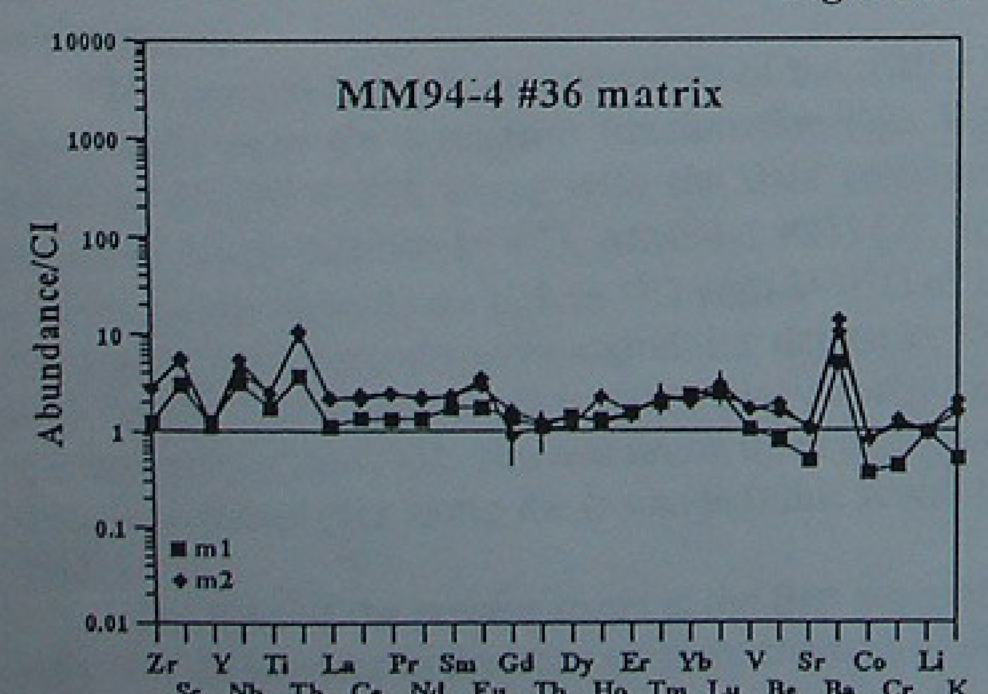

Figure 1c

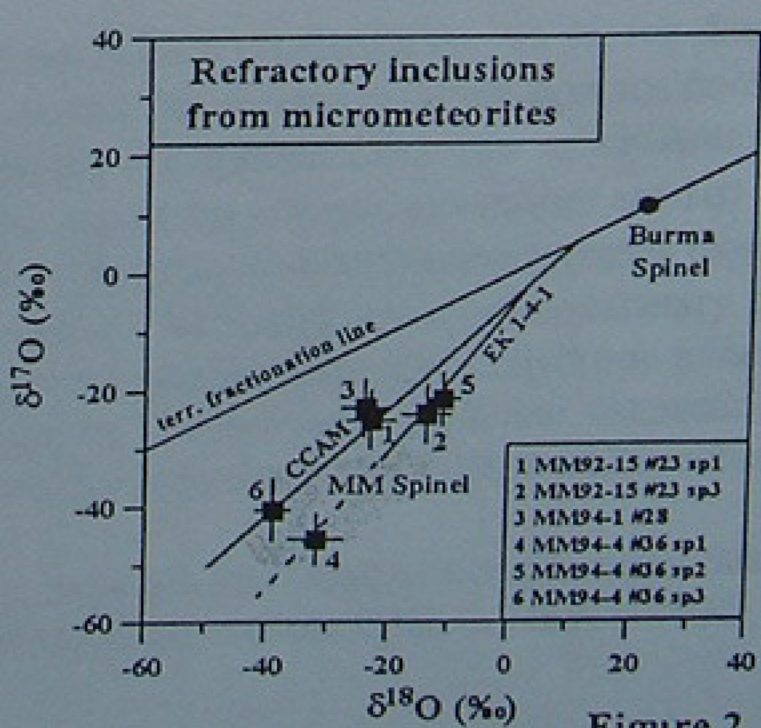

Figure 2